Algal Research 32 (2018) 79–92

Contents lists available at ScienceDirect

Algal Research

journal homepage: www.elsevier.com/locate/algal

Alterations in lipidome and metabolome profiles of *Nannochloropsis salina* in response to reduced culture temperature during sinusoidal temperature and light

Stephanie Willette[a], Saba S. Gill[a], Barry Dungan[a], Tanner M. Schaub[b], Jacqueline M. Jarvis[b], Rolston St. Hilaire[a], F. Omar Holguin[a,*]

[a] Department of Plant and Environmental Sciences, New Mexico State University, Las Cruces, Mexico
[b] Chemical Analysis and Instrumentation Laboratory, New Mexico State University, Las Cruces, Mexico

ARTICLE INFO

Keywords:
Eicosanpentaenoic acid (EPA)
Lipid remodeling
Nannochloropsis salina
Microalgae
Metabolomics
Total fatty acids

ABSTRACT

Metabolic response to four suboptimal cultivation temperatures was explored in *Nannochloropsis salina*, with an emphasis on fatty acid and lipid metabolism. Cultures were cultivated in controlled environmental photobioreactors. Physiological performance, characterized by growth rate and photosynthetic output, were reduced at all three cold stress temperatures (5 °C, 10 °C, 15 °C). However, biomass productivity and overall growth for cultures at 20 °C was like that of those grown at the optimal temperature (25 °C). Fatty acid productivity was elevated at all suboptimal temperatures, and both total fatty acid and eicosapentaenoic acid content were statically elevated at 20 °C. Lipid accumulation was observed exclusively in response to cold stress; however, lipid turnover and enrichment in polyunsaturated fatty acids occurred in all temperature variants. In addition, extensive lipid remodeling occurred in both polar and neutral lipid pools, specifically in monogalactosyl diacylglycerol and triacylglycerol pools. While 20 °C is optimal for eicosapentaenoic acid and total fatty acid productivity, cold stress is necessary to induce both productivity and polyunsaturated fatty acid enrichment in triacylglycerol pools.

1. Introduction

Over the past several decades, research initiatives have become increasingly devoted to increasing the availability and incorporation of essential fatty acids into the human diet [1–5]. Essential fatty acids include omega-6 (*n*-6) and omega-3 (*n*-3) fatty acids are precursors to eicosanoids, which serve as bioactive signaling molecules with several roles implicated in modulation of ion channels, hormone release, blot clotting factors, and immune response [6–10]. Omega-6 and -3 fatty acids are used to produce eicosanoids with pro- and anti-inflammatory effects, respectively; therefore, the ratio of *n*-6:*n*-3 fatty acids is an important consideration for human health [11–13]. Currently, the predominant dietary source of n-3 fatty acids is fish oil; however, large predatory fish bioaccumulate toxins from smaller fishes, in addition to oil from microalgae [14]. Therefore, microalgae are heavily studied to determine sustainability as potential feedstocks for aquacultures and other unexplored markets [12,14–16]. Most dietary fats are triglycerides; therefore, an ideal feedstock for omega fatty acids is one that produces TAGs that contain *n-3* fatty acid side-chains.

Algal species from *Isochyrsis*, *Nannochloropsis*, *Pavlova* and *Phaeodactylum* have been investigated for biomass and lipid productivity and omega fatty acid content [17–19]. Several species from *Nannochloropsis* are shown to be both oleaginous (up to 60% oil by dry weight) and naturally abundant in *n-3* eicosapentaenoic acid (EPA) [19,20]. Additional work has shown that oil and EPA production in *Nannochloropsis* sp., *N. gaditana*, *N. oceanica*, *N. oculata,* and *N. salina* can be elevated through abiotic perturbation, such as genetic manipulation [21–24], nitrogen starvation [25–31], altering light intensity [27–33], and by altering growing temperature conditions [31,34]. Several other studies have explored lipid metabolism and remodeling within different species of *Nannochloropsis*, and have shown that environmental perturbations, such as light intensity and nitrogen deprivation, result in lipid remodeling and TAG accumulation, respectively [19,32,35–39]. However, the regulatory mechanisms that underlie elevated productivity are usually not studied or discussed within *Nannochloropsis* sp.

In this study, *N. salina* was selected for its known increased EPA productivity under reduced temperature conditions, particularly under

* Correspondence author.
E-mail addresses: stephwi@nmsu.edu (S. Willette), sabagill@nmsu.edu (S.S. Gill), bdungan@nmsu.edu (B. Dungan), tschaub@nmsu.edu (T.M. Schaub), jmjarvis@nmsu.edu (J.M. Jarvis), rsthilai@nmsu.edu (R. St. Hilaire), frholgui@nmsu.edu (F. Omar Holguin).

https://doi.org/10.1016/j.algal.2018.03.001
Received 9 February 2017; Received in revised form 11 December 2017; Accepted 1 March 2018
Available online 26 March 2018

cold stress [31,34]. Periodic temperature and/or light variations induced metabolic variation without altering biomass productivity; therefore, a 12:12 h sinusoidal temperature regime and 14:10 h sinusoidal light regime were chosen to mitigate reduced growth rate in response to low cultivation temperatures [33,40]. Temperature variants included 5 °C, 10 °C, 15 °C and 20 °C, and a control temperature maintained at a constant of 25 °C. Sinusoidal cycles fluctuated between minimum temperatures and the optimal growth temperature (25 °C). Metabolomic and lipidomic profiles were collected for all temperatures, and compared to reveal roles for temperature modulation in pathways involved in carbon allocation, polyamine and energy metabolism. In addition, lipidomics data were organized by lipid class to determine the composition and relative abundance of glycolipids and neutral lipids. Metabolic and lipidomic data were integrated to reveal regulatory points and potential bottlenecks within lipid assembly and remodeling pathways, with an emphasis on PUFA movement between polar and neutral lipid pools.

2. Materials and methods

2.1. Cultivation and experimental growth

2.1.1. Batch cultures & inoculation

Nannochloropsis salina CCMP 1776 cultures were originally obtained from the Provasoli-Guillard Center for the Culture of Marine Phytoplankton (Bigelow, ME). Batch cultures were prepared using an 8-fold enriched f/2 medium [41] with 35 ppt salinity (Instant Ocean, VA). Cultures were maintained at 25 °C with a 16:8 h photoperiod at a photosynthetically active radiation (PAR) of 250 μmol photons $m^{-2} s^{-1}$. Supplemental CO_2 (1 ± 0.5%) was aerated into the incubator through silicone tubing, and pH values for batch cultures were maintained at 7.2 ± 0.3. Cellular suspension was maintained by storing cultures on an AROS 160 Thermolyne shaker table (Thermo Fisher, US) set at 90 rpm.

Batch cultures were grown for approximately 14 days, and inoculated in six environmental photobioreactors (ePBRs; Phenometrics, US) when cultures were confirmed to be in exponential growth phase ($\geq 0.11\ g\ L^{-1}\ d^{-1}$). Cultures were diluted in fresh f/2 medium to an optical density of 0.35 ± 0.025, determined using UV/Vis spectrophotometry (DU 530, Beckman Coulter, US) at a wavelength of 750 nm. Three experimental runs were performed using a randomized block design to represent biological triplicates of each temperature regime. Control temperature cultures were included in each experimental run resulting in n = 5, and one random temperature variant (15 °C, n = 4) was randomly selected and included in the third experimental run. All ePBRs were filled with an initial volume of 500 mL inoculum, and initial Algal Command setting were applied for 12 h: temperature control at 25 °C, sinusoidal light control set at a light intensity of 250 μmol photons $m^{-2} s^{-1}$, magnetic stirring at 300 rpm, and 1.0% CO_2 sparging at 7.0 mL min^{-1}. The first 12 h were maintained under control settings to confirm the health and exponential growth of each culture.

2.1.2. Experimental growth period & growth conditions

The cultures were incubated at 25 °C in the ePBRs for 12 h before adjusting to the target sinusoidal temperature conditions. Temperatures all ranged from a high of 25 °C to a low of three different cold stress temperatures: 15 °C, 10 °C or 5 °C. A control was maintained at a constant 25 °C through the growth period. Temperatures within the ePBRs varied within ± 2.0 °C throughout each experimental growth period. All ePBRs, including the control, were grown under sinusoidal light conditions with a 14:10 h photoperiod.

Daily sampling was performed 17 h into the photoperiod every 24 h based on preliminary hourly data which revealed that relative lipid content is highest 3 h into the night cycle of the photoperiod. Duplicate 2 mL aliquots were collected every 24 h throughout the 96 h growth period under reduced sinusoidal temperature conditions. Samples were measured to determine optical density, nutrient uptake, photosynthetic activity, relative total lipid content, and cellular replication. Cultures were harvested after 96 h growth, and centrifuged at 5000 rpm for 10 min. Supernatant was discarded, and all pellets were lyophilized at −43 °C under 10^{-3} mbar for 36 h then stored at −80 °C until further analysis.

2.1.3. Experimental statistics

All statistical data were prepared using Statistical Analysis System (SAS) University Edition, version 9.3 (JMP, US). Repeated measures analysis was performed on all physiological data that were collected throughout the growth period, and an ANCOVA was performed with the best-fitted covariance models. ANOVA was used to assess data sets containing single measurements. Statistical significance was determined for $P \leq 0.05$.

MetaboAnalyst V2.6.3 (Xia Laboratory, QC) was used to assess statistical information for metabolomics data [42]. Metabolic profiles were formatted for submission to the online platform *via* Excel, and subsequent analysis was performed online through MetaboAnalyst. MetaboAnalyst provides several statistical methodologies; however, only ANOVA data are shown here. P-values ≤ 0.05 were identified as significant.

2.2. Daily sampling procedures

2.2.1. Optical density and growth rate (d^{-1})

Optical density was measured daily using UV/Vis spectrophotometry (DU 530, Beckman Coulter, US). Measurement was taken at 750 nm for cell density, 680 nm for relative chlorophyll content, and 450 nm for relative carotenoid content. Cell density measurements recorded at 0 h and 96 h time points of the growth period were used to calculate the growth rate and doubling time for each temperature treatment. Measurements were averaged for biological triplicates (n = 3) for 20 °C, 10 °C and 5 °C, and biological replicates for 25 °C (n = 5) and 15 °C (n = 4). The following equations [43] were used to calculate (1) growth rate and (2) doubling time:

$$\text{Growth rate } (d^{-1}) = \frac{\ln OD_{4\,d} - \ln OD_{0\,d}}{4\,d} \quad (1)$$

$$\text{Doubling time (d)} = \frac{\ln 2}{\text{Growth rate}} \quad (2)$$

2.2.2. Pulse-amplitude modulation (PAM) chlorophyll fluorometry

Relative photosynthetic activity was recorded nightly using PAM chlorophyll fluorometry with Junior-PAM (Walz, Germany). Measurements included variable fluorescence (F_v), maximal fluorescence (F_m) and electron transport rate (ETR) values. Relative photosynthetic activity was determined between each temperature treatment over the 96 h growth period using the ratio of variable to maximal fluorescence (F_v/F_m). Triplicate measurements were collected for each culture with 30 s intervals between measures. Triplicate measurements were averaged for each sample, and subsequently averaged for each temperature condition (25 °C, n = 5; 20 °C, n = 3; 15 °C, n = 4; 10 °C, 5 °C, n = 3).

2.2.3. Dissolved oxygen

Dissolved oxygen measurements were collected every 24 h directly from each ePBR using a FireSting optical oxygen meter (Pyro Science, US). Dissolved oxygen was measured in parts per million (ppm) over a 30 s sampling duration. Measurements were collected every second, and all 30 measurements were averaged to estimate total dissolved oxygen. Dissolved oxygen values were then corrected for temperature by normalization to O_2 solubility by temperature. Values were then averaged for biological replicates (25 °C, n = 5; 20 °C, n = 3; 15 °C,

n = 4; 10 °C, 5 °C, n = 3).

2.2.4. Total cell count

Cell replication was determined by daily cell count measurements obtained with a Petroff-Hausser counting chamber by Brightfield microscopy with 100× magnification on a Zeiss Axioplan microscope (Zeiss, Germany). Samples were prepared by fixing 2 μL aliquots of culture sample onto the counting chamber, and cell counts were recorded in triplicate for each sample. Total cell counts were calculated using the following equation based on the counting chambers dimensions (0.25 mm l × 0.25 mm w × 0.02 mm d):

$$\text{Total cell count} = \left[\frac{\#\text{cells}}{0.25\ \text{mm} \times 0.25\ \text{mm} \times 0.02\ \text{mm}}\right] \times \left(\frac{1\ \text{mm}^3}{1\ \mu\text{L}}\right) \times \left(\frac{1000\ \mu\text{L}}{1\ \text{mL}}\right) \times \left(\frac{1000\ \text{mL}}{1\ \text{L}}\right) \quad (3)$$

Subsequently, total cell counts were then averaged for biological replicates (25 °C, n = 5; 20 °C, n = 3; 15 °C, n = 4; 10 °C, 5 °C, n = 3).

2.2.5. Nutrient assays

Nutrient uptake of total nitrate and phosphate was assessed daily from culture samples by a colorimetric microplate assay [44]. Samples were prepared from 2 mL aliquots, which were centrifuged at 10,000 rpm for 10 min to clear residual cells and debris. Supernatant was removed and diluted in deionized (DI) water for analysis: aliquots for phosphate analysis were diluted 1:4 and diluted 1:49 for nitrite/nitrate analysis. Additionally, 40 μM KNO_3, 50 μM $NaNO_2$ and 40 μM KH_2PO_4 were used as standards, and (8) serial dilutions of each were used to generate standard curves (Supplemental Fig. 1). Total nitrate content was determined indirectly: a background nitrite concentration is recorded, then nitrate is reduced to nitrite with a microplate nitrate redactor (ParaTechs, US). Nitrite, nitrate and phosphate content for each sample was calculated from the standard curves, after which values were averaged for biological replicates (25 °C, n = 5; 20 °C, n = 3; 15 °C, n = 4; 10 °C, 5 °C, n = 3). Total nitrate is then calculated by the subtraction of the nitrite background from total nitrite content reduced from nitrate.

2.2.6. Relative lipid quantitation

Relative total lipid content was measured daily to estimate relative change throughout the growth period and validate the duration of the experiment. An affordable, quick Nile red fluorescence microplate assay was used to evaluate relative differences between temperatures throughout the growth period [45]. Assays were prepared daily from 2 mL aliquots of culture samples in black, clear-bottom 96-well plates. Four replicates of each sample were used, and 250 μL aliquots were loaded into each well. Additionally, 25 μL of dimethyl sulfoxide (DMSO):f/2 medium and 25 μL of 50 μg/mL Nile red dye solution was added to each well to produce a final concentration of approximately 4 μg/mL Nile red. The DMSO treatment was prepared DMSO:f/2 medium (1:1 v/v).Microplates were shaken in darkness for 5 min, and then an initial absorbance measurement (600 nm) was recorded with a Synergy HT multi-detection microplate reader (BioTek, US). Then fluorescence was read with an excitation wavelength of 485/20 nm and a fluorescence emission wavelength of 528/20 nm. Fluorescence values were normalized with initial absorbance values, and then technical replicates (n = 4) were averaged for each sample. Finally, normalized fluorescence values were averaged for biological replicates (25 °C, n = 5; 20 °C, n = 3; 15 °C, n = 4; 10 °C, 5 °C, n = 3).

2.3. Elemental analysis and carbon to nitrogen ratio

An elemental analysis was performed to determine carbon and nitrogen content by combustion analysis with a 2400 Series II CHNS/O Analyzer (PerkinElmer, US). Samples were prepared by loading 1–3 mg of lyophilized tissue into tin wrappers, and were then placed into the analyzer for combustion. Triplicates were prepared from each culture ($9 \leq n \leq 15$), and data generated by the analyzer were collected from the software package EA Data Manager (PerkinElmer, US). Data collected from EA Data Manager were then transferred to Excel to calculate carbon-to-nitrogen (C:N) ratios.

2.4. Fatty acid methyl ester (FAME) determination

Fatty acid methyl ester analysis was performed on 5–10 mg lyophilized tissue. Briefly a 200 μL aliquot of chloroform:methanol (2:1 v/v) was added to the tissue in a 2 mL vial. The *trans*-esterification reaction was catalyzed with the addition of 300 μL of 0.6 M potassium hydroxide:methanol and placed in an HP50 shaker oven (Apollo, US) at 30 °C for 30 min. Triplicate extractions were performed for each culture ($9 \leq n \leq 15$), and the resulting transesterfied fatty acids were back extracted into 0.9 mL hexane with an internal standard solution (methyl tricosonate, C23:0, at 50 μg/mL). FAMEs were then separated and analyzed with a gas chromatography mass spectrometry (GC–MS) system composed of a 3800 Gas Chromatograph (Varian, US) and Saturn 2000R Mass Spectrometer (Varian, US), the instrument was operated with same chromatographic conditions previously described by Weena et al. [46]. External calibration was used to generate a standard curves from a serial diluted Supelco 37 Component FAME mix (Sigma-Aldrich, US) in methylene chloride. The resulting standard curves for each FAME species, and the internal standard (C23:0) were used to quantify peaks within samples.

2.5. Metabolomics

2.5.1. Metabolome extraction and analysis

Total metabolites were extracted from 5 to 10 mg lyophilized tissue into chloroform:methanol:water (10:3:1 v/v/v) and tissue was homogenized with 0.5 mm glass beads in a bead mill (BIOSPEC, US) for three cycles at 45 s each [47]. Samples were derivatized and analyzed within 24 h with a gas chromatography time of flight mass spectrometry (GC-TOF-MS) composed of a 7890A GC System (Agilent Technologies, US) and a Leco Pegasus HT High Throughput TOF-MS (Leco, US). Total ion chromatograms were deconvoluted with Chromatof 4.41 (Leco, US), and unique characteristic ions were quantified by peak area.

2.5.2. Metabolite identification and profiling

Spectral data for unique characteristic ions were search against the Fiehn metabolomics library in Chromatof 4.41, and were subsequently organized for relative quantitation in MET-IDEA V2.08 (Noble Foundation, US). Peak area was normalized to sample tissue weight, and $\log_2$ transformed for statistical and pathway enrichment analyses. Statistical analysis was performed with MetaboAnalyst 3.0, and ANOVA was used to determine statistical change in metabolite levels between temperature variants. In addition, a pathway enrichment analysis was performed by VANTED V2.6.3 with modified *Chlamydomonas reinhardtii* reference pathways from the Kyoto Encyclopedia of Genes and Genomes (KEGG) database. Universal reference pathways (Glycolysis, Tricarboxylic Acid Cycle, Fatty Acid Synthesis, Calvin-Bensom Cycle) were used and modified based on the level of coverage within a given pathway. While the microalga *C. reinhardtii* was chosen as a reference due to its relative similarity to *N. salina,* and has been used to model lipid metabolism in microalgae [48], the analysis focused on universal primary metabolism.

2.6. Lipidomics

Total lipids were extracted following the Folch method with few modifications [49]. Lyophilized tissue (15–25 mg) was homogenized with 0.5 mm glass beads in a bead mill for three cycles at 45 s each, and then extracted with a ratio of 1:20 volumes of chloroform:methanol

(2:1 v/v). Samples were then diluted 1:3 in chloroform:methanol:ispropanol (1:2:4 v/v/v), and 1 mL aliquots were designated for both positive and negative electrospray ionization (ESI). Aliquots were supplemented with 5 μL of either 1 M sodium acetate and LTQ/FT-Hybrid or 1 M ammonium hydroxide and LTQ/FT-Hybrid for positive and negative ESI, respectively. Intact lipids were analyzed as described by Holguin and Schaub with a Thermo-Finnigan hybrid linear ion trap Fourier transform ion cyclotron (FT-ICR) MS (LTQ FT, Thermo, US) equipped with an Advion Triversa NanoMate (Advion, US) as previously described [50–55]. With this approach, we utilize direct infusion of dilute lipid extract solutions and employ ultrahigh mass resolving power and sub-part-per-million *m/z* measurement accuracy to facilitate isotopic fine structure analysis, Kendrick mass sorting, and elemental composition determination. Mass spectral peak-picking was performed to include all signals with peak magnitudes > 20:1 signal-to-noise ratio. Mass spectra are internally calibrated using a range of known lipids present in the mixtures and or the addition ESI Positive or Negative calibration mix (Pierce, US). For dilute electrospray solutions as used here, ion suppression effects are not significant [56] and observed ion signals are directly proportional to solution phase concentration and provide a means to monitor fold-change differences for compounds between samples. In this case, comparison between compounds or classes of compounds within a single sample (quantitation) is not possible for a vast majority of due to the limited availability of analytical standards relative to the number of observed compounds and compound classes. Assigned elemental compositions are matched to an in-house assembled lipid library derived from Lipid Maps (http://www.lipidmaps.org/) for tentative lipid molecular assignment.

3. Results & discussion

3.1. Effects of sinusoidal cold stress on overall cell growth and photosynthetic activity

Cultures from all temperature regimes exhibited growth rates consistent with exponential growth in *N. salina* [19,34,57] throughout the 96 h growth period and, ranged from 6.2–8.5 d for cultures at 25 °C down to 5 °C, respectively (Table 1). These rates are calculated with Eqs. (1) and (2) from Section 2.2.1 and the OD values in Table 1. Growth data reveal a pattern of reduced performance in cultures under cold stress, while cultures grown at 20 °C perform similarly to those maintained at a constant 25 °C. Statistical differences are denoted by mean separation letters (A, B, C, D) which group treatments based on least squares mean values. Cold stress began to affect growth after 24 h, with statistical differences appearing for 5 °C cultures at 24 h and 10 °C and 15 °C cultures at 48 h (Supplemental Table 1a). In addition, cell proliferation decreased under reduced temperatures throughout time. Cell division rates in cultures under cold stress are decreased significantly in comparison to the control after 48 h, and decreased at 20 °C after 72 h (Supplemental Table 1a). Cell division mobilizes lipids to form nascent membranes in new cells; therefore, decreased cell division is expected to contribute to elevated lipid content.

The average F_v/F_m ratios were relatively consistent throughout time (± 0.031) and reveal no intuitive trends regarding performance; although, control cultures exhibit the highest average values, and the lowest averages are for cultures at 5 °C after 48 h (Table 1). Additionally, ETR values suggest reduced performance in cultures under cold stress (Table 1). Cultures grown at the suboptimal temperature (20 °C) did not undergo statistical alterations in photosynthetic activity (Supplemental Table 1b). Finally, normalized dissolved oxygen values also exhibited similar trends to PAM measurements (Table 1). Oxygen output is a direct measure of photosynthesis; therefore, its correlation to PAM data validates reduction in photosynthetic activity across temperatures. These data together suggest that cold stress induces significant downregulation in photosynthetic activity, yet cultures can withstand < 10 °C below optimal temperature without significant loss in photosynthetic activity.

Nutrient availability was examined to determine whether nutrient-limiting conditions were present in any temperature conditions throughout the growth period. Alterations in growth performance have similar implications on nutrient consumption, and the trend for nutrient uptake mirrors that of the other growth parameters: nutrient uptake is reduced as a function of time in temperature variants. Total nitrate removal ranges from 26.1% at 5 °C to 42.7% at 25 °C with respect to initial concentrations, and total phosphate ranges from 14.9% at 5 °C to 30.1% at 25 °C (Supplemental Table 2). These data suggest that the rate of nitrate uptake is higher than that of phosphate uptake in *N. salina*, and are supported by nitrate to phosphate ratios which decrease across all temperatures throughout the growth period. Statistical data show that ratios do not differ significantly between temperature variants over time (Supplemental Table 1c). These results suggest that *N. salina* can modulate internal nitrate and phosphate uptake at suboptimal temperatures.

3.2. Lipid accumulation and fatty acid profile

Normalized total lipid estimates based on the Nile red fluorescence assay was consistent between all cultures for the first measurement (0 h), and increased significantly throughout time (Supplemental Fig. 2). The greatest increase in relative total lipid estimates between temperatures was observed within the first 48 h, which was followed with a reduction in relative lipid accumulation across all temperature treatments. This suggests that the cold stress response occurs within the first 48 h, and cellular synchronicity begins to occur after 48 h under sinusoidal light and temperature control.

Fatty acid methyl esters (FAMEs) were quantified based on standard curves calculated from Supelco® 37 Component FAME Mix (Sigma, US), and concentration by dry cell weight (mg/g) was calculated for all primary fatty acids. Fatty acid species observed at a concentration of approximately 0.5 mg/g or greater are shown in Table 2. Palmitic, palmitoleic and *n*-3 eicosapentaenoic acids (C16:0; C16:1; EPA, C20:5) are the three dominant species observed for each temperature and correspond to what has been previously reported in *N. salina* [31,34,57]. The overall trend produced by these data is that the degree of desaturation is increased across all temperature variants for primary fatty acids. EPA content was enriched across all temperature variants except for 5 °C, which exhibits reduced EPA production in comparison to the control. Statistical data show that EPA is significantly enriched at 20 °C (59.38 mg/g) compared to 25 °C (31.68 mg/g), while stearic and oleic acids were significantly reduced at 5 °C. In addition, total fatty acid (TFA) content increased across all temperatures variants except for 5 °C, which may suggest that cold stress > 15 °C below optimal conditions has deleterious effects on fatty acid synthesis. Cultures at 20 °C produced the highest TFA (204.4 mg/g) compared to the control (157.0 mg/g), which was found to be statistically significant (see Supplemental Table 3). Cold stress moderately upregulates *de novo* fatty acid synthesis and subsequent modification in *N. salina*, while suboptimal temperature (20 °C) significantly elevates fatty acid and EPA production.

Fatty acid distribution was monitored across all temperatures. Total SFA content decreased with temperature, where that observed at 15 °C (32.88 mg/g) is significantly lower in comparison to the control (43.97 mg/g). Additionally, the proportion of SFA to TFA is shown to be significant at both 15 °C and 20 °C (0.177 and 0.193, respectively) compared to the control (0.285). For reduced temperature, there is significant increase in the abundance unsaturated fatty acid (UFA), and PUFA compounds across all temperature variants, including 5 °C. MUFAs however were not found to differ statistically between temperatures, which suggests that the ratio of palmitic and palmitoleic acids (C16:0, C16:1) is maintained across all temperatures. However, statistical alterations were observed for UFA at 10 °C (135 mg/g), 15 °C (142 mg/g) and 20 °C (165 mg/g) compared to the control (113 mg/g),

Table 1
Growth parameters for *Nannochloropsis salina* between temperature regimes over 96 h growth period. Optical density measurements (750 nm) and F_v/F_m values for all temperature variants collected every 24 h over the 4 day growth period. Values are averaged from biological replicates ($3 \leq n \leq 5$). Average growth rates and doubling times are also provided. In addition, total cell counts are included and values are averaged from technical triplicates ($9 \leq n \leq 15$), and dissolved oxygen values are averaged from 30 replicate reads ($90 \leq n \leq 150$). ± SE values and mean separation letters are provided for each data set.

Growth parameters for *Nannochloropsis salina* between temperature regimes over 4 d growth period

Growth rate determined through optical density (750 nm)

(°C)	0		1		2		3		4	
	Time (d)									
25	0.356 ± 0.005	A	0.452 ± 0.012	A	0.519 ± 0.009	A	0.538 ± 0.012	A	0.561 ± 0.012	A
20	0.356 ± 0.000	A	0.442 ± 0.002	A	0.502 ± 0.008	A	0.528 ± 0.007	A	0.540 ± 0.006	A
15	0.356 ± 0.005	A	0.435 ± 0.013	B	0.485 ± 0.006	B	0.499 ± 0.010	B	0.520 ± 0.009	B
10	0.356 ± 0.003	A	0.427 ± 0.017	B	0.465 ± 0.011	C	0.488 ± 0.003	B	0.515 ± 0.011	B
5	0.356 ± 0.003	A	0.426 ± 0.015	B	0.463 ± 0.023	C	0.474 ± 0.009	B	0.492 ± 0.006	B

Growth parameters for *Nannochloropsis salina* between temperature regimes over 4 d growth period

Growth rate (d^{-1}) and doubling time (d)

	25 °C	20 °C	15 °C	10 °C	5 °C
GR (d^{-1})	0.113 ± 0.003	0.100 ± 0.003	0.096 ± 0.005	0.096 ± 0.004	0.082 ± 0.001
DT (d)	6.183 ± 0.197	6.959 ± 0.186	7.283 ± 0.422	7.257 ± 0.333	8.451 ± 0.114

Growth parameters for *Nannochloropsis salina* between temperature regimes over 4 d growth period

(°C)	0		1		2		3		4	
	Total Cell Count (cells L^{-1})									
25	$1.0 \cdot 10^{10} \pm 6.7 \cdot 10^{8}$	A	$1.4 \cdot 10^{10} \pm 8.9 \cdot 10^{8}$	A	$1.7 \cdot 10^{10} \pm 1.1 \cdot 10^{9}$	A	$2.1 \cdot 10^{10} \pm 1.4 \cdot 10^{9}$	A	$2.4 \cdot 10^{10} \pm 1.7 \cdot 10^{9}$	A
20	$9.3 \cdot 10^{9} \pm 5.5 \cdot 10^{8}$	A	$1.1 \cdot 10^{10} \pm 7.9 \cdot 10^{8}$	A	$1.4 \cdot 10^{10} \pm 7.9 \cdot 10^{8}$	A	$1.6 \cdot 10^{10} \pm 8.8 \cdot 10^{8}$	B	$1.9 \cdot 10^{10} \pm 1.2 \cdot 10^{9}$	B
15	$1.0 \cdot 10^{10} \pm 9.2 \cdot 10^{8}$	A	$1.2 \cdot 10^{10} \pm 4.8 \cdot 10^{8}$	A	$1.4 \cdot 10^{10} \pm 4.7 \cdot 10^{8}$	B	$1.5 \cdot 10^{10} \pm 8.3 \cdot 10^{8}$	B	$1.7 \cdot 10^{10} \pm 9.1 \cdot 10^{8}$	B
10	$9.5 \cdot 10^{9} \pm 4.5 \cdot 10^{8}$	A	$1.2 \cdot 10^{10} \pm 7.3 \cdot 10^{8}$	A	$1.2 \cdot 10^{10} \pm 4.6 \cdot 10^{8}$	C	$1.5 \cdot 10^{10} \pm 3.6 \cdot 10^{8}$	B	$1.7 \cdot 10^{10} \pm 4.2 \cdot 10^{8}$	B
5	$1.1 \cdot 10^{10} \pm 7.1 \cdot 10^{8}$	A	$1.1 \cdot 10^{10} \pm 9.4 \cdot 10^{8}$	A	$1.2 \cdot 10^{10} \pm 8.6 \cdot 10^{8}$	C	$1.4 \cdot 10^{10} \pm 4.8 \cdot 10^{8}$	B	$1.5 \cdot 10^{10} \pm 5.9 \cdot 10^{8}$	B
	Maximal to variable chlorophyll fluorescence ratios (F_v/F_m)									
25	0.533 ± 0.006	A	0.548 ± 0.005	A	0.558 ± 0.005	A	0.563 ± 0.008	A	0.555 ± 0.004	A
20	0.538 ± 0.009	A	0.524 ± 0.008	A	0.555 ± 0.008	A	0.536 ± 0.014	A	0.543 ± 0.006	A
15	0.522 ± 0.006	A	0.520 ± 0.005	A	0.547 ± 0.006	A	0.534 ± 0.009	A	0.542 ± 0.004	B
10	0.520 ± 0.008	A	0.543 ± 0.007	A	0.549 ± 0.007	A	0.538 ± 0.012	A	0.535 ± 0.005	C
5	0.536 ± 0.008	A	0.540 ± 0.007	A	0.518 ± 0.007	B	0.524 ± 0.012	B	0.523 ± 0.005	C
	ETR (μmol electrons $m^{-2} s^{-1}$) values									
25	21.75 ± 2.32	A	19.38 ± 2.09	A	17.34 ± 0.98	A	18.83 ± 0.97	A	19.68 ± 1.18	A
20	24.62 ± 3.53	A	19.65 ± 3.44	A	17.53 ± 1.61	A	15.89 ± 1.60	A	22.21 ± 1.94	A
15	17.77 ± 2.40	A	17.37 ± 2.34	A	16.33 ± 1.09	A	14.81 ± 1.09	B	12.77 ± 1.32	B
10	15.35 ± 2.98	A	14.18 ± 2.92	A	12.90 ± 1.36	B	13.30 ± 1.35	C	12.95 ± 1.65	B
5	17.00 ± 2.97	A	15.91 ± 2.90	A	14.06 ± 1.36	A	13.21 ± 1.35	C	11.63 ± 1.64	B
	Normalized dissolved oxygen									
25	0.614 ± 0.001	AB	0.607 ± 0.008	A	0.611 ± 0.004	A	0.599 ± 0.003	A	0.616 ± 0.005	A
20	0.564 ± 0.004	AB	0.584 ± 0.004	A	0.588 ± 0.002	AB	0.590 ± 0.002	AB	0.589 ± 0.003	B
15	0.606 ± 0.066	A	0.626 ± 0.048	A	0.560 ± 0.005	BC	0.556 ± 0.003	BC	0.562 ± 0.002	B
10	0.567 ± 0.103	AB	0.644 ± 0.074	A	0.544 ± 0.013	C	0.531 ± 0.004	C	0.534 ± 0.002	C
5	0.535 ± 0.077	B	0.599 ± 0.062	A	0.473 ± 0.019	D	0.468 ± 0.021	D	0.488 ± 0.012	D

and for PUFA at 20 °C (86.39 mg/g) compared to 25 °C (49.55 mg/g). Additionally, the overall proportion of UFA to TFA was significant at 15 °C (0.81) and 20 °C (0.82) compared to the control (0.72), and PUFA to TFA was significant at 15 °C (0.40) and 20 °C (0.44) compared to the control (0.30). These alterations suggest that the level of desaturation is elevated at suboptimal temperature. While desaturation was observed to increase with reduced temperature, fatty acid synthesis was elevated at 15 °C and 20 °C only. This suggests that the mechanisms by which synthesis, elongation and desaturation are affected separately by suboptimal temperature *vs.* cold stress.

3.3. Elemental analysis

Elemental analysis was performed to quantitate carbon, hydrogen, nitrogen and sulfur content to determine whether global alterations in carbon and nitrogen occurred at suboptimal temperatures. Carbon-to-nitrogen (C:N) ratios were calculated from raw scores (Table 3). Minor alterations were observed: nitrogen increased at all temperatures compared to the control, while carbon increased at 15 °C and 20 °C only. Therefore, C:N ratios were found to favor nitrogen at all suboptimal temperatures. These data suggest that production of nitrogen-rich species, such as RNA and protein, is elevated at suboptimal temperature. A reduction in photosynthetic activity at suboptimal temperature likely reduces the rate of carbon fixation relative to nitrogen assimilation. The implications of elevated cellular carbon and nitrogen are reflected in the metabolic profiles of cultures grown at suboptimal temperatures.

Table 2
Fatty acid profiles for N. salina under five temperature regimes. Fatty acid concentration (mg/g) in dry cell weight for primary fatty acids found in *N. salina* between temperature variants. Concentrations are calculated and averaged from biological and technical triplicates ($9 \leq n \leq 15$), and standard error values are provided. Abbreviations: total fatty acid (TFA), saturated fatty acid (SFA), unsaturated fatty acid (UFA), monounsaturated fatty acid (MUFA), polyunsaturated fatty acid (PUFA).

Temperature (°C)					
Fatty acids	25	20	15	10	5
C14:0	5.86 ± 0.85	3.92 ± 1.41	3.55 ± 0.96	5.64 ± 1.19	3.65 ± 1.19
C16:0	35.57 ± 2.57	34.38 ± 4.23	28.19 ± 2.88	38.36 ± 3.58	32.37 ± 3.57
C16:1	57.26 ± 4.62	73.31 ± 7.62	66.16 ± 5.18	62.17 ± 6.45	67.16 ± 6.42
C16:2	1.57 ± 0.26	1.53 ± 0.16	1.49 ± 0.24	1.38 ± 0.30	0.91 ± 0.91
C16:3	0.43 ± 0.06	0.56 ± 0.10	0.41 ± 0.07	0.33 ± 0.09	0.27 ± 0.09
C18:0	2.54 ± 1.14	0.50 ± 1.88	1.15 ± 1.28	4.66 ± 1.59	1.75 ± 1.59
C18:1	6.20 ± 0.66	5.93 ± 1.09	5.07 ± 0.74	3.80 ± 0.92	1.92[b] ± 0.92
C18:2	2.75 ± 0.23	3.28 ± 0.38	2.61 ± 0.26	1.92 ± 0.32	1.64[a] ± 0.32
C18:3 *n*-3	1.14 ± 0.26	1.41 ± 0.42	0.66 ± 0.29	0.60 ± 0.36	0.72 ± 0.36
C20:3 *n*-3	2.00 ± 0.37	2.64 ± 0.61	1.55 ± 0.41	1.62 ± 0.51	1.12 ± 0.51
C20:3 *n*-6	5.08 ± 0.77	2.88 ± 1.27	3.96 ± 0.86	5.97 ± 1.07	4.64 ± 1.07
C20:4 *n*-6	6.46 ± 2.68	16.25 ± 4.41	12.68 ± 3.00	11.69 ± 3.74	12.79 ± 3.72
C20:5 *n*-3	31.68 ± 6.28	59.38[a] ± 10.37	49.06 ± 7.05	46.42 ± 8.77	29.96 ± 8.74
TFA	156.98 ± 7.12	204.42[b] ± 11.75	175.04 ± 7.99	183.17 ± 9.95	158.00 ± 9.91
% TFA	15.70 ± 0.70	20.44[b] ± 1.16	17.50 ± 0.79	18.32 ± 0.98	15.80 ± 0.97
ΣSFA	43.97 ± 3.09	38.80 ± 5.10	32.88[b] ± 3.47	48.65 ± 4.32	37.77 ± 4.30
ΣUFA	113.00 ± 5.64	165.60[c] ± 9.32	142.20[b] ± 6.33	134.50[a] ± 7.88	120.20 ± 7.85
ΣMUFA	63.46 ± 4.49	79.24 ± 7.37	71.23 ± 5.01	65.97 ± 6.24	69.08 ± 6.22
ΣPUFA	49.55 ± 6.48	86.39[a] ± 10.70	70.93 ± 7.28	68.54 ± 9.06	51.15 ± 9.02
ΣSFA/TFA	0.28 ± 0.01	0.18[c] ± 0.02	0.19[c] ± 0.01	0.27 ± 0.02	0.24 ± 0.02
ΣUFA/TFA	0.72 ± 0.01	0.82[b] ± 0.02	0.81[c] ± 0.02	0.73 ± 0.02	0.76 ± 0.02
ΣPUFA/TFA	0.30 ± 0.02	0.44[b] ± 0.04	0.40[a] ± 0.02	0.38 ± 0.03	0.32 ± 0.03
ΣPUFA/UFA	0.43 ± 0.03	0.53 ± 0.05	0.49 ± 0.03	0.51 ± 0.04	0.42 ± 0.04
ΣMUFA/PUFA	1.46 ± 0.21	0.85 ± 0.34	1.12 ± 0.23	1.00 ± 0.29	1.47 ± 0.29

[a] $P < 0.05$.
[b] $P < 0.01$.
[c] $P < 0.001$.

Table 3
Elemental analysis for Nannochloropsis salina under five temperature regimes. Elemental values (% wt) for carbon and nitrogen (sulfur and hydrogen not provided). All values are averaged from biological replicates and technical triplicates ($9 \leq n \leq 15$), and ± SE values are provided.

Temperature (°C)					
Elemental sp.	25	20	15	10	5
C:N	6.84 ± 0.08	6.70 ± 0.14	6.58 ± 0.09	6.66 ± 0.12	6.71 ± 0.12
Carbon	40.47 ± 0.46	41.20 ± 0.76	41.03 ± 0.52	39.70 ± 0.64	40.29 ± 0.64
Nitrogen	5.92 ± 0.07	6.15 ± 0.125	6.24[a] ± 0.08	5.98 ± 0.10	6.01 ± 0.11

[a] $P < 0.05$.

3.4. Metabolomics

Metabolomics data were collected and peak areas were normalized to sample tissue weight, then $\log_2$ transformed. Normalized, transformed data were mapped to modified KEGG pathways using VANTED V2.6.3, and 33 metabolites involved in central metabolism and fatty acid synthesis were identified (Supplemental Fig. 3). *t*-Tests were performed on the ratio of temperature variant to control in VANTED, and revealed a statistical difference for at least one temperature in 32/33 metabolites and differences in all temperature variants for 6/33 metabolites. Of the six metabolites that fluctuate under sinusoidal temperature control, two are tricarboxylic acid (TCA) cycle intermediates: fumarate and acetyl coenzyme A (acetyl CoA).

At lower temperatures, acetyl CoA pools are likely diverted for fatty acid synthesis, elongation and transport. Acetyl-CoA and NADPH supplies have been shown to be limiting factors in lipid productivity in *N. salina* under mixotrophic growth conditions [58]. Therefore, the global acetyl-CoA pool is expected to be low when carbon allocation events, such as fatty acid and lipid assembly, are upregulated by environmental stress. However, α-ketoglutarate was the only other TCA cycle intermediate found to be depleted (Fig. 1). Metabolic and proteomic profiles for other microalgal species have shown that nitrogen deprivation upregulates the TCA cycle [59,60]. Anaplerotic reactions regenerate several central metabolites, such as oxaloacetate and α-ketoglutarate, which are regenerated from aspartate and glutamate, respectively. Oxaloacetate and aspartate levels were up- and down-regulated respectively at suboptimal temperatures; however, α-ketoglutarate and glutamate exhibited the opposite relationship. These results suggest that α-ketoglutarate is not recovered at the same rate as other TCA cycle intermediates, or serves as an intermediate for a separate metabolic pathway.

Most of the intermediates involved in fatty acid synthesis are heat labile, and therefore were not detected in the metabolomics survey; however, several free fatty acids (FFAs) were successfully quantitated and mapped in Fig. 2. Palmitoleic acid (C16:1) was elevated at suboptimal temperature, yet palmitic acid (C16:0) was increased only at 15 °C. Additionally, arachidonic and eicosanoic acids were both elevated at 15 °C only, and oleic and linoleic acids were decreased at 10 °C, 15 °C and 20 °C. Alterations in FFA levels for specific species suggest that elongation and desaturation activity may also be modulated by temperature.

In addition, the normalized, transformed metabolomes for all temperature conditions were statistically analyzed using MetaboAnalyst 3.0, and organized based on compound class. Supplemental Table 4

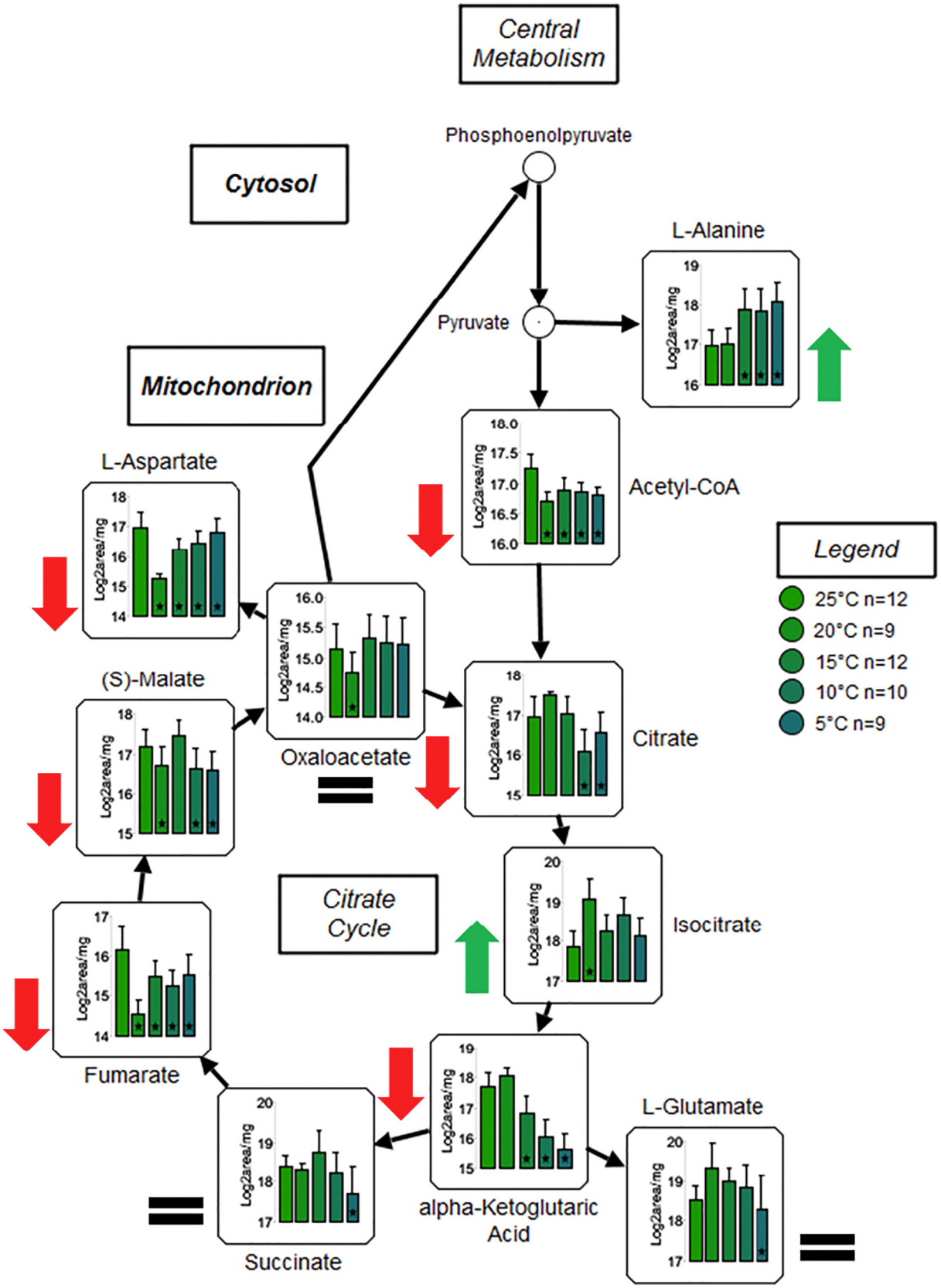

Fig. 1. Abbreviated pathway map for citrate cycle. Undetected metabolites are represented by open circles. Graphs represent $\log_2$ transformed data; values are averaged from biological triplicates and technical replicates ($9 \leq n \leq 12$). Range values are 13–22, bars represent ± SE values, and stars denote statistical significance ($\alpha = 0.05$). Arrows and equal signs are used to denote upregulation (green arrow), downregulation (red arrow) and no statistical change (equal sign) for metabolites of interest. (For interpretation of the references to color in this figure legend, the reader is referred to the web version of this article.)

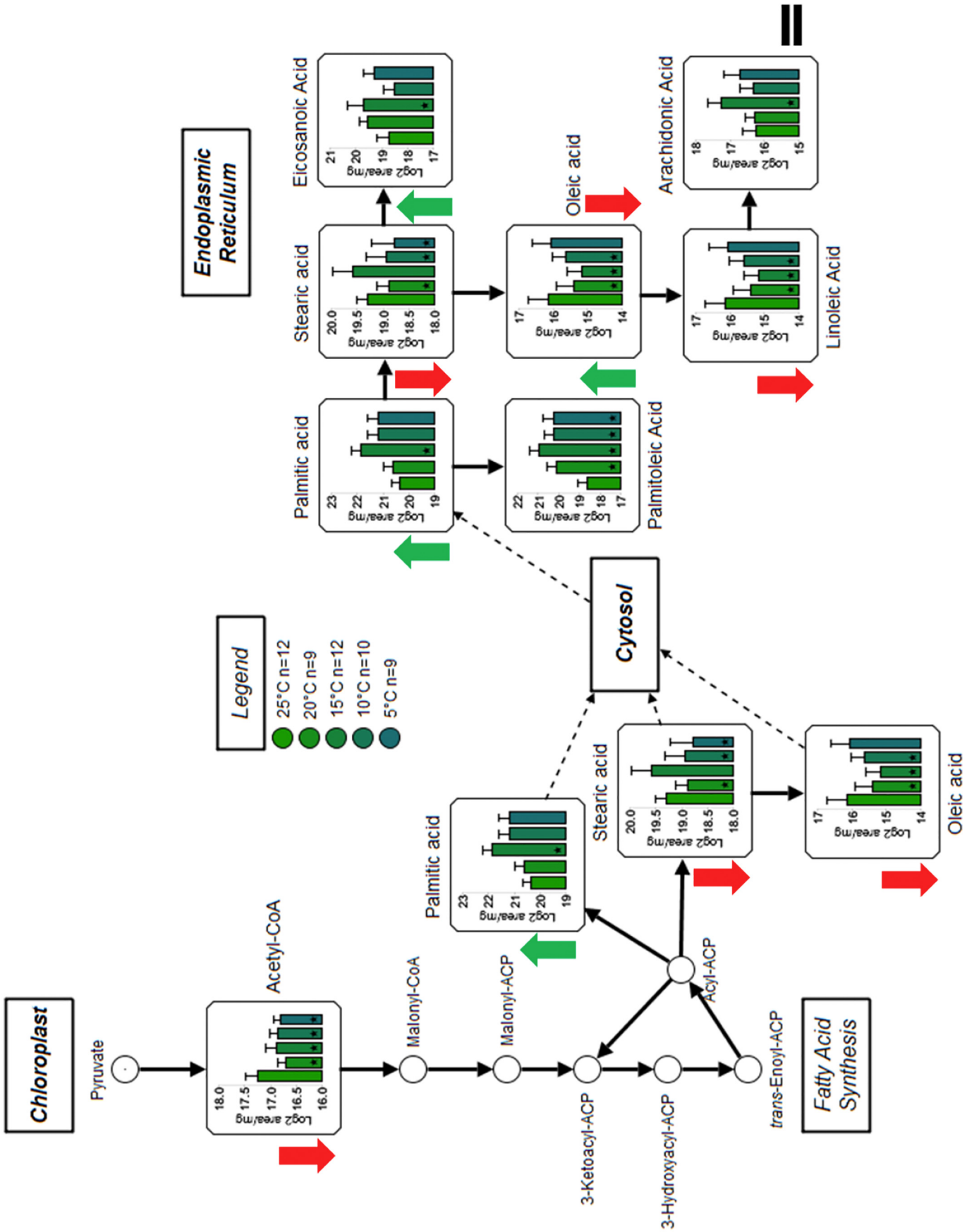
Chloroplast
Pyruvate
Acetyl-CoA
Malonyl-CoA
Malonyl-ACP
3-Ketoacyl-ACP
3-Hydroxyacyl-ACP
trans-Enoyl-ACP
Acyl-ACP
Fatty Acid Synthesis
Palmitic acid
Stearic acid
Oleic acid
Cytosol
Endoplasmic Reticulum
Palmitic acid
Stearic acid
Eicosanoic Acid
Palmitoleic Acid
Oleic acid
Linoleic Acid
Arachidonic Acid
Legend
25°C n=12
20°C n=9
15°C n=12
10°C n=10
5°C n=9
Log2 area/mg

Fig. 2. Abbreviated global pathway map for fatty acid synthesis, transport, elongation and desaturation. Undetected metabolites are represented by open circles. Graphs represent $\log_2$ transformed data; values are averaged from biological triplicates and technical replicates ($9 \leq n \leq 12$). Range values are 13–22, bars represent ± SE values, and stars denote statistical significance ($\alpha = 0.05$). Arrows and equal signs are used to denote upregulation (green arrow), downregulation (red arrow) and no statistical change (equal sign) for metabolites of interest. (For interpretation of the references to color in this figure legend, the reader is referred to the web version of this article.)

contains 10 compound classes across 4 tables: organic and fatty acids (a), amino acids and derivatives (b), carbohydrates (c), and N-containing compounds (d). Statistical analysis reveals that 26 of the 106 categorized compounds are present at significantly altered levels across the temperature variants, including α-ketoglutarate, γ-aminobutyric acid (GABA), and several mono- and poly-saccharides. GABA is known to be an important signaling molecular involved in stress response in higher plants [61], and is also intimately associated with the citrate cycle as a shunt pathway that generates succinate from glutamate, which can be diverted back into the citrate cycle. Succinic acid is produced through the shunt pathway, and both GABA and succinic acid were statistically elevated at suboptimal temperature (Supplemental Table 4a). Additionally, α-ketoglutarate was depleted while glutamate levels were stable, which suggests that α-ketoglutarate undergoes amination to maintain glutamate levels when the shunt pathway is active.

The most statistically significant alterations were observed in amino acid and amino acid derivative profiles. While proline has been shown to increase at higher temperatures [62], it is found to be increased across all temperature regimes in this study (Supplemental Table 4b). Both cysteinylglycine and glutamate are increased across all cold stress variants, which implicates glutathione degradation; however, glutathione was not detected in the metabolomics survey. Alanine was enriched at all suboptimal temperatures, and isoleucine, valine and serine increased slightly. Tryptophan quantity between temperatures exhibited the greatest variability, with no apparent trend in response to cold stress. *N*-Acetylornithine was shown to be significantly reduced under cold stress, which suggests downregulation of arginine synthesis.

Carbohydrates are divided into four subgroups: phosphorylated sugars, sugar alcohols and acids, and saccharides. Isomaltose, maltose and melibiose are shown to be significantly enriched at 5 °C, and glucose and mannose are significantly enriched at 15 °C (Supplemental Table 4c). Cold stress in spinach was shown to induce elevated production of several soluble sugars [63]. Most saccharides varied over a dynamic range between temperatures. Glycerol was consistent, yet glycerol 3-phosphate - the first metabolite in *de novo* TAG biosynthesis - was depleted at suboptimal temperature. Phosphorylated sugars involved in the Calvin cycle were decreased at lower temperatures; however, 3-phosphoglycerate an intermediate of both the Calvin cycle and glycolysis increased significantly under cold stress.

Polyamine metabolism has been investigated in higher plants under cold stress, and shown that increased polyamines are siphoned into pathways associated with defense mechanisms [63,64]. Putrescine was upregulated in cultures under cold stress, while spermine levels remained relatively low across all temperatures (Supplemental Table 4d). Spermidine and spermine are both acetylated to serve as substrates for oxidases, and downstream transaminases that generate precursors to both *β*-Alanine and GABA, respectively [61]. When the GABA shunt pathway is upregulated, spermine will be consumed for anaplerotic reactions. Spermine levels were numerically reduced at lower temperatures; however, no statistical differences were reported from MetaboAnalyst. These results suggest that polyamine metabolism is involved in the stress response in *N. salina* during cold stress.

3.5. Lipidomics

Several lipid classes were identified, along with numerous species within each class, within total intact lipid extracts that were analyzed by FT-ICR-MS in both positive and negative electrospray ionization modes. Negative ionization mode was utilized to detect phosphorylated and sulfonated lipid species with deprotonated adducts ($[M\text{-}H]^-$), which included phosphatidyl diacylglycerol (PG), and sulfoquinovosyl diacylglycerol (SQDG). Positive ionization mode scanned for neutral and polar lipids containing sodium adducts ($[M + Na]^+$) including: triacylglycerols (TAGs), diacylglycerols (DAGs), mono- and di-galactosyl diacylglycerol (MGDG, DGDG), monogalactosyl monoacylglycerol (MGMG), and mono- and di-acylglycerol trimethyl-homoserine (MGTS, DGTS). Analysis of the raw spectra identified over 90 lipid species, 67 of which were selected for analysis. Molecular formulae, adducts and *m/z* values are provided for all lipids analyzed (Supplemental Table 5). Signals generated for each lipid species were representative of peak area, and were normalized to sample weight for each sample. Sum totals for all lipid species within a given class were used to calculate relative abundance (%) for each lipid species, and determine species distribution for each lipid class. Individual lipid speciation is designated by respective number of carbon and double bonds ([Acyl C:DBE]) found in the acylated portion of each lipid. The acylated portion is calculated by the subtraction of glyceride and respective head groups from the total elemental composition of each lipid.

Sum peak area for each lipid class was used to calculate fold change between the treatments *vs.* control to determine relative differences in total production within each lipid class (Table 4). Relative increases were observed for most lipid groups at 5 °C and 10 °C; however, it should be noted that sum peak area may not be compared between lipid classes due to differences in ionization efficiency between lipid classes. Most notably, the monoacylated groups MGTS and MGMG were elevated under cold stress. Membrane lipids are often assembled from DAG; therefore, the monoacylated products are more likely derived from degradation processes [56,65]. The presence of monoacylglycerols within membrane lipid groups suggests that these groups likely participate in lipid remodeling. Species distribution within monoacylated lipid groups may also provide information regarding lipid remodeling; specifically, which fatty acids are more likely to be retained or recycled. This suggests that cold stress (> 10 °C below optimal) likely drives lipid remodeling and movement of existing PUFA, over *de novo* fatty acid and lipid synthesis pathways.

3.6. Betaine Lipids

Prior work has shown that DGTS compounds are targeted for lipid

Table 4
Fold change heat map for lipid classes under five temperature treatments. Sum totals for primary lipid pools in *N. salina* calculated from sum S/N values for species within each lipid class. S/N values above a threshold limitation of 20 were selected and normalized to dry cell weight. Values were averaged for sample replicates (n = 3), and fold change was calculated by the ratio of treatment values to the average control value.

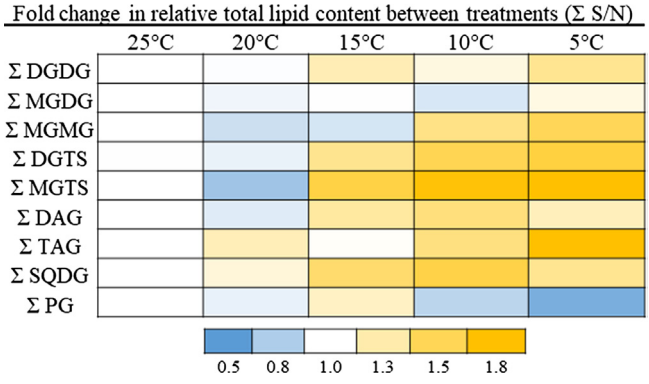

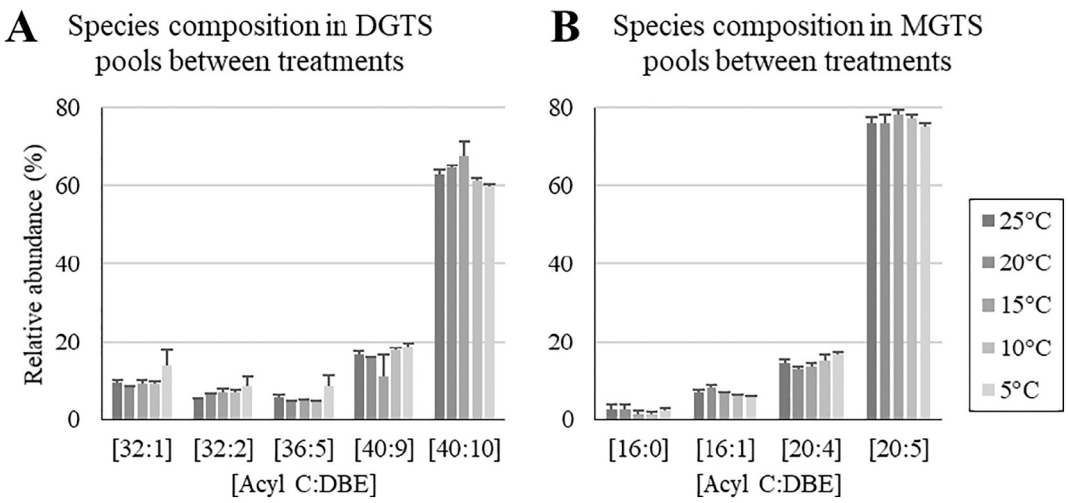

Fig. 3. Acyl carbon and unsaturation distribution present in betaine lipid profiles across all temperature treatments: a) diacylglycerol tri-methylhomoserine (DGTS) and b) monoacylglycerol tri-methylhomoserine (MGTS). The x-axis title [Acyl C:DBE] represents the number of carbons and double bonds present in the side-chains for a given lipid species. Relative abundance (%) was calculated from S/N values acquired from positive ESI. Values are averaged from biological replicates from three repeated experiments (n = 3), ± SE bars are shown.

remodeling earlier than other lipids [56,65], which is supported by the presence of the monoacylated product, MGTS. Both DGTS and MGTS were elevated in cold-stress cultures (Table 4). The presence of both lipid groups at elevated abundance suggests that both DGTS production and turnover are induced by cold stress. Additionally, elevated DGTS content has been observed under other stress conditions in *N. gaditana*, which suggests that this lipid class participates in a cellular stress response in several *Nannochloropsis* species [32].

Further, alterations were observed in the species composition of DGTS and MGTS pools, specifically ARA- and EPA-containing species (Fig. 3). Three of the five most abundant DGTS species detected contain ARA and EPA, and two of those species were elevated in cold-stressed cultures. Both C40:9 and C40:10 species were found to be statistically abundant at 15 °C (Supplemental Table 6). These results correspond to Alboresi et al., which also reported a moderate and high relative abundance of ARA and EPA in DGTS, respectively [32]. Other work has shown that DGTS profiles in *N. salina* may also be rich in monounsaturated species (C32:1, C32:2) [53]. These species were also detected; however, no statistical alterations were observed for these species in cold-stress cultures. MGTS pools primarily contain ARA and EPA species; however, the C16:0 species was statistically low at 15 °C, which suggests that PUFA are preferentially retained in betaine lipids during remodeling.

3.7. Di- and tri-acylglycerols

Neutral lipids have no assumed functional role, and are thought to serve as storage units for excess carbon; however, both DAG and TAG pools underwent dynamic alterations during reduced temperature, which suggests a potential role in cellular stress response. Overall DAG and TAG productivity was increased in cold-stressed cultures (Table 4). Additionally, TAG production was statistically elevated at both 10 °C and 5 °C (Supplemental Table 6). Other environmental stress conditions, such as altered nutrient and light conditions, have been shown to induce neutral lipid production in different species of *Nannochloropsis* [32,66,67]. Accumulation within DAG and TAG pools may result from increased contribution from either remodeling or *de novo* pathways. Reduced temperature also resulted in changes in species composition within both DAG and TAG pools (Fig. 4). Both primary species in DAG pools (C32:2, C40:10) were elevated at reduced temperatures, while several polyunsaturated TAG species were elevated, including C46:2, C48:Δ, C56:10. C56:11, and C60:15 (Δ = 2–5). Half of the TAG species selected for analysis (12/24) were statistically altered at reduced temperatures compared to optimal (25 °C) (Supplemental Table 6). However, the relative abundance for C40:9 and C40:10 at 15 °C were the only statistical differences observed in DAG. These data suggest that it is unlikely that TAG assembly is driven solely by *de novo* synthesis *via* the glycerol 3-phosphate/Kennedy pathway.

Overall, the degree of desaturation for both DAG and TAG was elevated at suboptimal temperature. This observation was also supported by the FAME analysis, which showed that UFA and PUFA were statistically elevated at suboptimal temperatures. While EPA-rich (C60:15) TAG was detected at a very low relative abundance, the lipid species was enriched in cold-stressed cultures (up to 1.77% at 10 °C) relative to the control (0.94%). EPA-rich DAG (C40:10) was also enriched at suboptimal temperature, which validates the presence and relative abundance of EPA-rich TAG. These results suggest that EPA is likely remodeled into DAG and TAG pools from betaine lipids over *de novo* synthesis and assembly of EPA-rich DAG and TAG at reduced culture temperature.

3.8. Glycolipids

Thylakoid membranes in microalgae are primarily composed of MGDG, DGDG, SQDG and PG [17,35,68]. MGDG and DGDG pools have been characterized for several species of *Nannochloropsis*, and have been proposed to contain an obligate proportion of C32:Δ, C34:Δ and C36:Δ species (Δ = 0–7) [69–72]. MGDG turnover may produce either DGDG or MGMG, both of which are detected in *N. salina* at all temperature conditions. Both DGDG and MGMG levels were elevated in cold-stressed cultures, while MGDG levels were relatively stable at all temperatures (Table 4). Galactolipids have been shown to be depleted under altered light intensity and reduced nitrogen conditions [32,66,67,71]. However, at reduced temperature elevated galactolipid productivity is proposed to mitigate cold stress effects on thylakoid structure through increased membrane fluidity [73–75]. This is supported by an increased relative abundance of C40:10 observed in MGDG pools at all reduced culture temperatures (Fig. 5A). PUFA enrichment has been associated with stress response at reduced temperatures in other microalgae and diatoms [73,74]. In addition, photosynthetic measurements (F_v/F_m, ETR and O_2) provide a basis for identifying chloroplastic damage in response to reduced temperature conditions. The relationship between reduced photosystem II efficiency and enriched PUFA content suggest that *N. salina* modulates thylakoid membrane fluidity through lipid remodeling pathways.

Other MGDG species were relatively stable at reduced temperatures; however, C32:1 and C32:2 were depleted. These monounsaturated species are likely converted to DGDG, which had a high relative

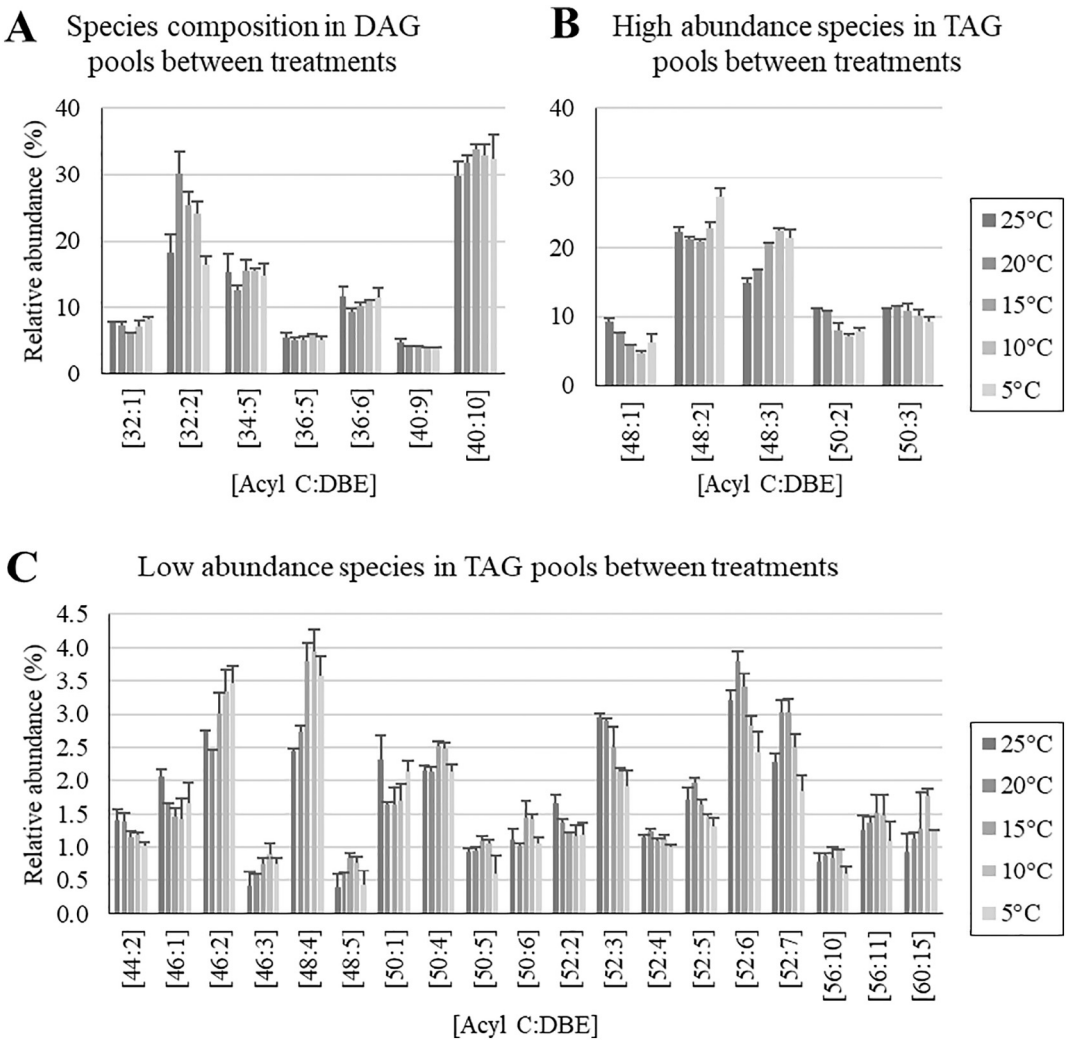

Fig. 4. Acyl carbon and unsaturation distribution present in neutral lipid profiles across all temperature treatments: a) diacylglycerol (DAG), b) high relative abundance (> 5%) triacylglycerol (TAG), and c) low relative abundance (< 5%) TAG. The x-axis title [Acyl C:DBE] represents the number of carbons and double bonds present in the side-chains for a given lipid species. Relative abundance (%) was calculated from S/N values acquired from positive ESI. Values are averaged from biological replicates from three repeated experiments (n = 3), ± SE bars are shown.

abundance of both species (Fig. 5B). All other species detected in both MGDG and DGDG were shown to be relatively constant at reduced temperatures, which suggests that cold stress does not affect which species are selected for MGDG turnover to DGDG. Additionally, two MGMG species were detected (Fig. 5C). A small proportion of a MGMG product containing EPA was detected, which suggests that MGDG retains a basal level of EPA during lipid remodeling. This is supported by the statistical analysis, which reveals that EPA-rich MGDG (C40:10) is statistically elevated at all reduced temperatures (Supplemental Table 6). Additionally, MGDG C32:1 was found to be statistically depleted at all temperatures, which suggests that the proportion of MGDG species favors polyunsaturated species under reduced temperature conditions. This trend is also observed, to a lesser extent, in DGDG pools at cold stress temperatures. DGDG C34:5 was statistically elevated in cold-stressed cultures (Supplemental Table 6). While no statistical alterations were observed for the two MGMG species detected, significant differences were observed in MGDG for the distribution of species C32:1 and C40:10, which suggests that reduced cultivation temperature affects MGDG assembly. Additionally, reduced temperature was shown to affect MGDG turnover, which is represented by statistical differences observed in DGDG profiles during cold stress (Supplemental Table 6).

Like the galactolipids, PG contains both monounsaturated and polyunsaturated species (Fig. 5D). However, both polyunsaturated species (C36:5 and C36:7) detected for PG were depleted at reduced temperatures. Statistical analysis revealed significant depletions in C36:7 at both 15 °C and 5 °C (Supplemental Table 6). PG is able to be converted into DAG; however, fluxes of C36:5 and C36:7 in DAG were not observed and no monoacylated form of PG was detected. This suggests that reduced temperature may reduce PUFA-rich PG production, which is supported by reduced overall PG levels observed at 10 °C and 5 °C (Table 4). Additionally, polar thylakoid lipids have been implicated in cellular signaling processes [68], which may explain why trends in PG and SQDG species composition and distribution differ from MGDG and DGDG in response to reduced culture temperature.

Relative SQDG levels were elevated at all reduced temperature (Table 4). In addition, alterations were observed in all SQDG species in response to reduced temperature (Fig. 6). Most notably, the primary SQDG species (C32:1) was depleted by at least 10% at all reduced temperatures (Fig. 6A). Low abundance species, such as C34:5 and C34:6, were observed at a higher abundance in cold-stressed cultures. The proportion of polyunsaturated species was shown to increase, which suggests that SQDG also contributes to membrane fluidity during reduced temperature conditions. SQDG has been implicated in cellular signaling between chloroplastic and cytosolic proteins, and also for its contribution to protein orientation and structure, and peptide transport in higher plants [76]. Additionally, work in several species of

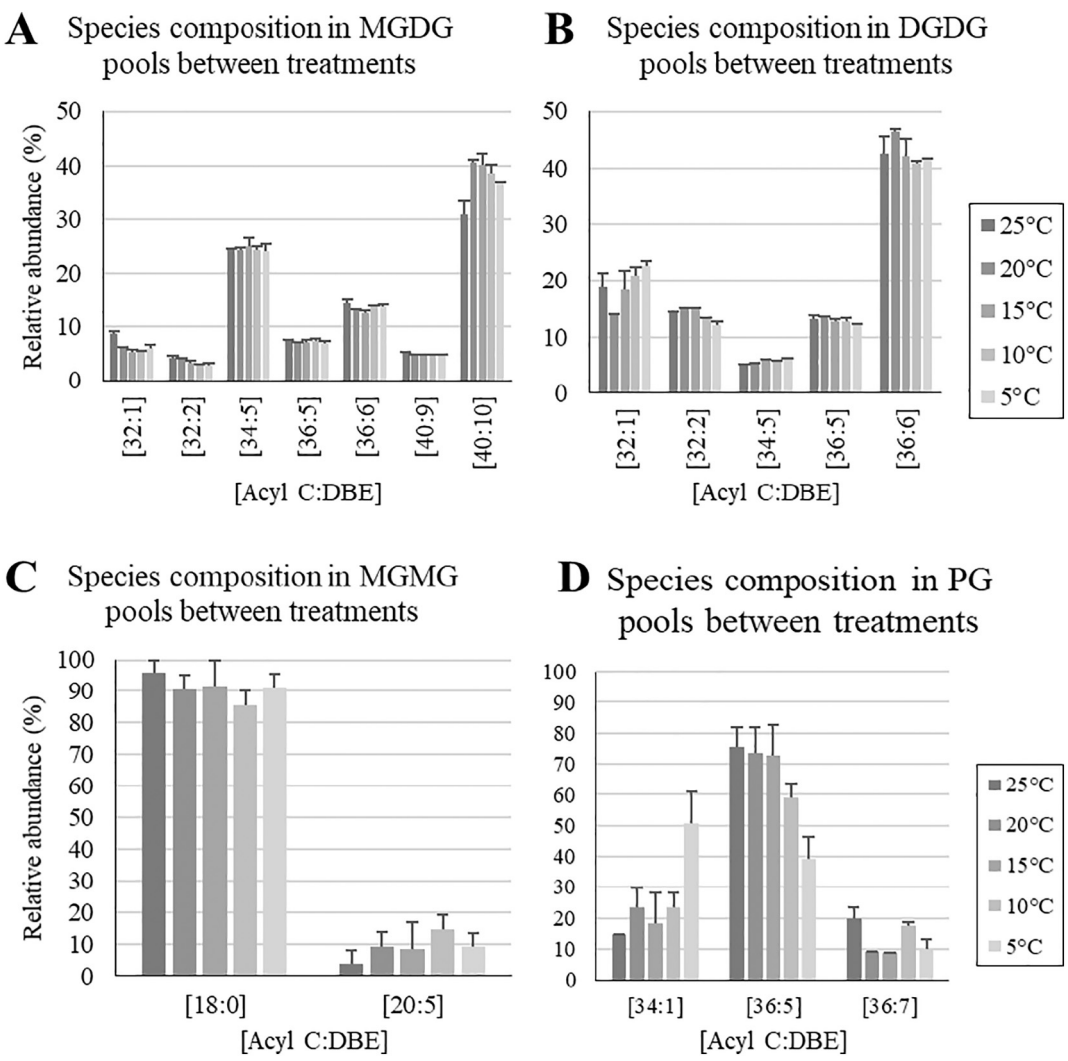

Fig. 5. Acyl carbon and unsaturation distribution present in galacto- and glycerophospho- lipid profiles across all temperature treatments: a) monogalactosyl diacylglycerol (MGDG), b) digalactosyl diacylglycerol (DGDG), c) monogalactosyl monoacylglycerol (MGMG), and d) phosphatidylglycerol (PG). The x-axis title [Acyl C:DBE] represents the number of carbons and double bonds present in the side-chains for a given lipid species. Relative abundance (%) is calculated from S/N values acquired from positive ESI. Values are averaged from biological replicates from three repeated experiments (n = 3), ± SE bars are shown.

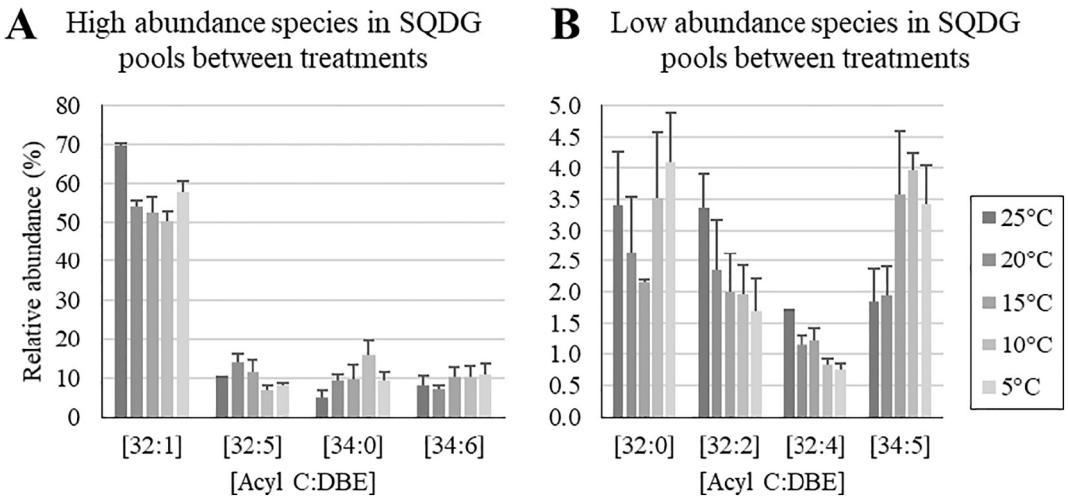

Fig. 6. Acyl carbon and unsaturation distribution present in sulfo lipid profiles across all temperature treatments: a) high relative abundance (> 5%) sulfoquinovosyl diacylglycerol (SQDG), and b) low relative abundance (< 5%) SQDG. The x-axis title [Acyl C:DBE] represents the number of carbons and double bonds present in the side-chains for a given lipid species. Relative abundance (%) is calculated from S/N values acquired from negative ESI. Values are averages from biological replicates from three repeated experiments (n = 3), ± SE bars are shown.

cyanobacteria has shown that both MGDG and SQDG accumulate in cold-stressed cultures [77–79]. These results illustrate that thylakoid lipid metabolism is mediated by a highly coordinated set of pathways that are tightly modulated by environmental changes. MGDG, DGDG and SQDG all showed relative increases in the proportion of polyunsaturated species in response to reduced temperature. However, cold stress produced varied effects on the overall relative levels within each lipid group. This indicates a need for further investigation to explore signaling pathways and secondary metabolism associated with the different thylakoid lipid groups.

4. Conclusions

Biomass productivity is reduced by cold stress over a 4-day cultivation period that results in a maximum reduction of 27.4% at 5 °C and minimum of 11.5% at 20 °C compared to optimal (25 °C) based on growth rate. However, the loss in overall biomass production is less dynamic than what has been observed during constant reduced cultivation temperature, and validates that sinusoidal temperature control produces less deleterious effects on growth and physiology. In addition, only cultures at 20 °C exhibited statistically elevated levels of both TFA and EPA. Sustainable, elevated fatty acid synthesis is possible at 20 °C because damage to the thylakoid is minimal in comparison to cold stress condition. LC-PUFA synthesis is therefore optimal within 10 °C of the optimal growth temperature (25 °C).

Alterations in global primary metabolite pools were also observed in all temperature variants, especially in citrate cycle intermediates. These alterations in the citrate cycle suggest upregulation in anabolism and biosynthetic pathways, such as fatty acid synthesis and lipid assembly. Shunt pathways involved in anaplerosis, such as γ-aminobutyric acid, and polyamine metabolism were upregulated in response to cold stress, and are sufficient to regenerate succinate in all temperature variants. Suboptimal temperature also produced downstream consequences for lipid assembly and turnover, specifically the degree of desaturation and accumulation in membrane and neutral lipids pools.

Highly polyunsaturated species were detected in all lipid classes, and were found at an elevated relative abundance in DAG, TAG, DGTS/MGTS and MGDG/MGMG groups in cultures grown at reduced temperature, which suggests that reduced temperature induces pathways associated with LC-PUFA transport and assimilation between these lipid groups. Elevated levels of both MGTS and MGMG support that temperature induces lipid remodeling in DGTS and MGDG. These two lipid groups are integral to cellular and chloroplastic structure; therefore, remodeling within these groups during environmental perturbation is likely associated with cell survival. However, lipid remodeling of LC-PUFA in neutral lipids, specifically TAG, has no current known biological functional or structural purpose [73–75]. One proposed function for lipid droplets is to provide electron sinks for reactive oxygen species (ROS) generated during photosynthetic processes [35,36]. However, photosynthetic processes were downregulated in cultures grown at reduced temperatures, which suggests that ROS production would also be diminished. Additional investigation into alterations at the proteomic level will be required to elucidate potential roles for LC-PUFA assimilation in lipid bodies.

Author contribution

SW, SSG, RSH and FOH conceived and designed the research; SW and SSG conducted experiments; SW, SSG, BD, JMJ and TMS analyzed and interpreted data. SW and FOH wrote the manuscript. All authors read and approved the manuscript.

Acknowledgements

This research project was funded under National Institutes of Health (NIH) SC2 award Project: HL126060 and National Science Foundation (NSF) award #IIA-1301346.

Appendix A. Supplementary data

Supplementary data to this article can be found online at https://doi.org/10.1016/j.algal.2018.03.001.

References

[1] A.H. Lichtenstein, L.J. Appel, M. Brands, M. Carnethon, S. Daniels, H.A. Franch, B. Franklin, P. Kris-Etherton, W.S. Harris, B. Howard, Diet and lifestyle recommendations revision 2006, Circulation 114 (2006) 82–96.
[2] J. Dyerberg, H. Bang, E. Stoffersen, S. Moncada, J. Vane, Eicosapentaenoic acid and prevention of thrombosis and atherosclerosis? Lancet 312 (1978) 117–119.
[3] L. Frøyland, H. Bentsen, I. Graff, M. Myhrstad, J. Paulsen, K. Retterstøl, Evaluation of Negative and Positive Health Effects of N-3 Fatty Acids as Constituents of Food Supplements and Fortified Foods, Opinion of the Steering Committee of the Norwegian Scientific Committee for Food Safety, Norwegian Scientific Committee for Food Safety (VKM), Oslo, Norway, 2011.
[4] J.R. Hibbeln, L.R. Nieminen, T.L. Blasbalg, J.A. Riggs, W.E. Lands, Healthy intakes of n − 3 and n − 6 fatty acids: estimations considering worldwide diversity, Am. J. Clin. Nutr. 83 (2006) S1483–1493S.
[5] N.D. Riediger, R.A. Othman, M. Suh, M.H. Moghadasian, A systemic review of the roles of n-3 fatty acids in health and disease, J. Am. Diet. Assoc. 109 (2009) 668–679.
[6] P.C. Calder, Polyunsaturated fatty acids and inflammatory processes: new twists in an old tale, Biochimie 91 (2009) 791–795.
[7] C.D. Funk, Prostaglandins and leukotrienes: advances in eicosanoid biology, Science 294 (2001) 1871–1875.
[8] T.A. Jacobson, Secondary prevention of coronary artery disease with omega-3 fatty acids, Am. J. Cardiol. 98 (2006) 61–70.
[9] G. Michal, D. Schomburg, Biochemical Pathways: An Atlas of Biochemistry and Molecular Biology, Wiley, New York, 1999.
[10] J.G. Robinson, N.J. Stone, Antiatherosclerotic and antithrombotic effects of omega-3 fatty acids, Am. J. Cardiol. 98 ((2006) 39–49.
[11] P.B. Adams, S. Lawson, A. Sanigorski, A.J. Sinclair, Arachidonic acid to eicosapentaenoic acid ratio in blood correlates positively with clinical symptoms of depression, Lipids 31 (1996) S157–S161.
[12] E.B. Schmidt, J.H. Christensen, I. Aardestrup, T. Madsen, S. Riahi, V.E. Hansen, H.A. Skou, Marine n-3 fatty acids: basic features and background, Lipids 36 (2001) S65–S68.
[13] A.P. Simopoulos, The importance of the omega-6/omega-3 fatty acid ratio in cardiovascular disease and other chronic diseases, Exp. Biol. Med. 233 (2008) 674–688.
[14] S. Haas, J. Bauer, A. Adakli, S. Meyer, S. Lippemeier, K. Schwarz, C. Schulz, Marine microalgae *Pavlova viridis* and *Nannochloropsis* sp. as n-3 PUFA source in diets for juvenile European sea bass (*Dicentrarchus labrax* L.), J. Appl. Phycol. 28 (2016) 1011–1021.
[15] G.L. Ginsberg, B.F. Toal, Quantitative approach for incorporating methylmercury risks and omega-3 fatty acid benefits in developing species-specific fish consumption advice, Environ. Health Perspect. 117 (2009) 267.
[16] K.R. Mahaffey, R.P. Clickner, R.A. Jeffries, Methylmercury and omega-3 fatty acids: co-occurrence of dietary sources with emphasis on fish and shellfish, Environ. Res. 107 (2008) 20–29.
[17] A. Mühlroth, K. Li, G. Røkke, P. Winge, Y. Olsen, M.F. Hohmann-Marriott, O. Vadstein, A.M. Bones, Pathways of lipid metabolism in marine algae, co-expression network, bottlenecks and candidate genes for enhanced production of EPA and DHA in species of Chromista, Mar. Drugs 11 (2013) 4662–4697.
[18] V. Patil, T. Källqvist, E. Olsen, G. Vogt, H.R. Gislerød, Fatty acid composition of 12 microalgae for possible use in aquaculture feed, Aquac. Int. 15 (2007) 1–9.
[19] Y. Ma, Z. Wang, C. Yu, Y. Yin, G. Zhou, Evaluation of the potential of 9 *Nannochloropsis* strains for biodiesel production, Bioresour. Technol. 167 (2014) 503–509.
[20] Q. Hu, M. Sommerfeld, E. Jarvis, M. Ghirardi, M. Posewitz, M. Seibert, A. Darzins, Microalgal triacylglycerols as feedstocks for biofuel production: perspectives and advances, Plant J. 54 (2008) 621–639.
[21] N.K. Kang, S. Jeon, S. Kwon, H.G. Koh, S.-E. Shin, B. Lee, G.-G. Choi, J.-W. Yang, B.-r. Jeong, Y.K. Chang, Effects of overexpression of a bHLH transcription factor on biomass and lipid production in *Nannochloropsis salina*, Biotechnol. Biofuels 8 (2015) 200.
[22] C.-Y. Chen, Y.-C. Chen, H.-C. Huang, C.-C. Huang, W.-L. Lee, J.-S. Chang, Engineering strategies for enhancing the production of eicosapentaenoic acid (EPA) from an isolated microalga *Nannochloropsis oceanica* CY2, Bioresour. Technol. 147 (2013) 160–167.
[23] O. Kilian, C.S. Benemann, K.K. Niyogi, B. Vick, High-efficiency homologous recombination in the oil-producing alga *Nannochloropsis* sp, Proc. Natl. Acad. Sci. 108 (2011) 21265–21269.
[24] F. Li, D. Gao, H. Hu, High-efficiency nuclear transformation of the oleaginous marine *Nannochloropsis* species using PCR product, Biosci. Biotechnol. Biochem. 78 (2014) 812–817.
[25] J. Camacho-Rodríguez, A. González-Céspedes, M. Cerón-García, J. Fernández-Sevilla, F. Acién-Fernández, E. Molina-Grima, A quantitative study of eicosapentaenoic acid (EPA) production by *Nannochloropsis gaditana* for aquaculture as a

function of dilution rate, temperature and average irradiance, Appl. Microbiol. Biotechnol. 98 (2014) 2429–2440.
[26] A. Converti, A.A. Casazza, E.Y. Ortiz, P. Perego, M. Del Borghi, Effect of temperature and nitrogen concentration on the growth and lipid content of *Nannochloropsis oculata* and *Chlorella vulgaris* for biodiesel production, Chem. Eng. Process. Process Intensif. 48 (2009) 1146–1151.
[27] C.W. Kim, M.-G. Sung, K. Nam, M. Moon, J.-H. Kwon, J.-W. Yang, Effect of monochromatic illumination on lipid accumulation of *Nannochloropsis gaditana* under continuous cultivation, Bioresour. Technol. 159 (2014) 30–35.
[28] D. Pal, I. Khozin-Goldberg, Z. Cohen, S. Boussiba, The effect of light, salinity, and nitrogen availability on lipid production by *Nannochloropsis* sp, Appl. Microbiol. Biotechnol. 90 (2011) 1429–1441.
[29] A. Solovchenko, A. Lukyanov, O. Solovchenko, S. Didi-Cohen, S. Boussiba, I. Khozin-Goldberg, Interactive effects of salinity, high light, and nitrogen starvation on fatty acid and carotenoid profiles in *Nannochloropsis oceanica* CCALA 804, Eur. J. Lipid Sci. Technol. 116 (2014) 635–644.
[30] A. Sukenik, Y. Carmeli, T. Berner, Regulation of fatty acid composition by irradiance level in the eustigmatophyte *Nannochloropsis* sp, J. Phycol. 25 (1989) 686–692.
[31] J. Van Wagenen, T.W. Miller, S. Hobbs, P. Hook, B. Crowe, M. Huesemann, Effects of light and temperature on fatty acid production in *Nannochloropsis salina*, Energy 5 (2012) 731–740.
[32] A. Alboresi, G. Perin, N. Vitulo, G. Diretto, M.A. Block, J. Jouhet, A. Meneghesso, G. Valle, G. Giuliano, E. Maréchal, Light remodels lipid biosynthesis in *Nannochloropsis gaditana* by modulating carbon partitioning between organelles, Plant Physiol. 171 (2016) 2468–2482.
[33] B. Tamburic, S. Guruprasad, D.T. Radford, M. Szabó, R.M. Lilley, A.W. Larkum, J.B. Franklin, D.M. Kramer, S.I. Blackburn, J.A. Raven, The effect of diel temperature and light cycles on the growth of *Nannochloropsis oculata* in a photobioreactor matrix, PLoS One 9 (2014) e86047.
[34] M. Hoffmann, K. Marxen, R. Schulz, K.H. Vanselow, TFA and EPA productivities of *Nannochloropsis salina* influenced by temperature and nitrate stimuli in turbidostatic controlled experiments, Mar. Drugs 8 (2010) 2526–2545.
[35] Z.-Y. Du, C. Benning, Triacylglycerol accumulation in photosynthetic cells in plants and algae, Lipids in Plant and Algae Development, Springer, 2016, pp. 179–205.
[36] B. Liu, A. Vieler, C. Li, A.D. Jones, C. Benning, Triacylglycerol profiling of microalgae *Chlamydomonas reinhardtii* and *Nannochloropsis oceanica*, Bioresour. Technol. 146 (2013) 310–316.
[37] S.S. Merchant, J. Kropat, B. Liu, J. Shaw, J. Warakanont, TAG, You're it! Chlamydomonas as a reference organism for understanding algal triacylglycerol accumulation, Curr. Opin. Biotechnol. 23 (2012) 352–363.
[38] D. Simionato, M.A. Block, N. La Rocca, J. Jouhet, E. Maréchal, G. Finazzi, T. Morosinotto, The response of *Nannochloropsis gaditana* to nitrogen starvation includes de novo biosynthesis of triacylglycerols, a decrease of chloroplast galactolipids, and reorganization of the photosynthetic apparatus, Eukaryot. Cell 12 (2013) 665–676.
[39] A. Taleb, J. Pruvost, J. Legrand, H. Marec, B. Le-Gouic, B. Mirabella, B. Legeret, S. Bouvet, G. Peltier, Y. Li-Beisson, Development and validation of a screening procedure of microalgae for biodiesel production: application to the genus of marine microalgae *Nannochloropsis*, Bioresour. Technol. 177 (2015) 224–232.
[40] H. Bonnefond, N. Moelants, A. Talec, O. Bernard, A. Sciandra, Concomitant effects of light and temperature diel variations on the growth rate and lipid production of *Dunaliella salina*, Algal Res. 14 (2016) 72–78.
[41] R.R. Guillard, Culture of phytoplankton for feeding marine invertebrates, Culture Of Marine Invertebrate Animals, Springer, 1975, pp. 29–60.
[42] J. Xia, D.S. Wishart, Using metaboanalyst 3.0 for comprehensive metabolomics data analysis, Curr. Protoc. Bioinformatics (2016) 91 (14.10. 11-14.10).
[43] F. Widdel, Theory and measurement of bacterial growth, Di dalam Grundpraktikum Mikrobiologie, 4 2007.
[44] J. Hernández-López, F. Vargas-Albores, A microplate technique to quantify nutrients ($NO2-$, $NO3-$, $NH4+$ and $PO4^{3-}$) in seawater, Aquac. Res. 34 (2003) 1201–1204.
[45] I. Sitepu, L. Ignatia, A. Franz, D. Wong, S. Faulina, M. Tsui, A. Kanti, K. Boundy-Mills, An improved high-throughput Nile red fluorescence assay for estimating intracellular lipids in a variety of yeast species, J. Microbiol. Methods 91 (2012) 321–328.
[46] W. Sitthithanaboon, H.K. Reddy, T. Muppaneni, S. Ponnusamy, V. Punsuvon, F. Holguim, B. Dungan, S. Deng, Single-step conversion of wet *Nannochloropsis gaditana* to biodiesel under subcritical methanol conditions, Fuel 147 (2015) 253–259.
[47] D.Y. Lee, O. Fiehn, High quality metabolomic data for *Chlamydomonas reinhardtii*, Plant Methods 4 (2008) 7.
[48] J.J. Park, H. Wang, M. Gargouri, R.R. Deshpande, J.N. Skepper, F.O. Holguin, M.T. Juergens, Y. Shachar-Hill, L.M. Hicks, D.R. Gang, The response of *Chlamydomonas reinhardtii* to nitrogen deprivation: a systems biology analysis, Plant J. 81 (2015) 611–624.
[49] J. Folch, M. Lees, G. Sloane Stanley, A simple method for the isolation and purification of total lipids from animal tissues, J. Biol. Chem. 226 (1957) 497–509.
[50] M.L. Bartley, W.J. Boeing, B.N. Dungan, F.O. Holguin, T. Schaub, pH effects on growth and lipid accumulation of the biofuel microalgae *Nannochloropsis salina* and invading organisms, J. Appl. Phycol. 26 (2014) 1431–1437.
[51] E. Christensen, N. Sudasinghe, K.P.R. Dandamudi, R. Sebag, T. Schaub, L.M. Laurens, Rapid analysis of microalgal triacylglycerols with direct-infusion mass spectrometry, Energy Fuel 29 (2015) 6443–6449.
[52] B. Gašparović, A. Penezić, R.S. Lampitt, N. Sudasinghe, T. Schaub, Free fatty acids, tri-, di-and monoacylglycerol production and depth-related cycling in the Northeast Atlantic, Mar. Chem. 186 (2016) 101–109.
[53] F.O. Holguin, T. Schaub, Characterization of microalgal lipid feedstock by direct-infusion FT-ICR mass spectrometry, Algal Res. 2 (2013) 43–50.
[54] S. Negi, A.N. Barry, N. Friedland, N. Sudasinghe, S. Subramanian, S. Pieris, F.O. Holguin, B. Dungan, T. Schaub, R. Sayre, Impact of nitrogen limitation on biomass, photosynthesis, and lipid accumulation in *Chlorella sorokiniana*, J. Appl. Phycol. 28 (2016) 803–812.
[55] N. Sudasinghe, H. Reddy, N. Csakan, S. Deng, P. Lammers, T. Schaub, Temperature-dependent lipid conversion and nonlipid composition of microalgal hydrothermal liquefaction oils monitored by Fourier transform ion cyclotron resonance mass spectrometry, BioEnergy Res. 8 (2015) 1962–1972.
[56] X. Han, R.W. Gross, Shotgun lipidomics: electrospray ionization mass spectrometric analysis and quantitation of cellular lipidomes directly from crude extracts of biological samples, Mass Spectrom. Rev. 24 (2005) 367–412.
[57] S. Boussiba, A. Vonshak, Z. Cohen, Y. Avissar, A. Richmond, Lipid and biomass production by the halotolerant microalga *Nannochloropsis salina*, Biomass 12 (1987) 37–47.
[58] S. Bellou, G. Aggelis, Biochemical activities in *Chlorella* sp. and *Nannochloropsis salina* during lipid and sugar synthesis in a lab-scale open pond simulating reactor, J. Biotechnol. 164 (2013) 318–329.
[59] V. Rai, M. Muthuraj, M.N. Gandhi, D. Das, S. Srivastava, Real-time iTRAQ-based proteome profiling revealed the central metabolism involved in nitrogen starvation induced lipid accumulation in microalgae, Sci. Rep. 7 (2017).
[60] K.W.M. Tan, H. Lin, H. Shen, Y.K. Lee, Nitrogen-induced metabolic changes and molecular determinants of carbon allocation in *Dunaliella tertiolecta*, Sci. Rep. 6 (2016) 37235.
[61] K. Gupta, A. Dey, B. Gupta, Plant polyamines in abiotic stress responses, Acta Physiol. Plant. 35 (2013) 2015–2036.
[62] M. Cvikrová, L. Gemperlová, J. Dobrá, O. Martincová, I.T. Prásil, J. Gubis, R. Vanková, Effect of heat stress on polyamine metabolism in proline-over-producing tobacco plants, Plant Sci. 182 (2012) 49–58.
[63] Y.-E. Yoon, S. Kuppusamy, K.M. Cho, P.J. Kim, Y.-B. Kwack, Y.B. Lee, Influence of cold stress on contents of soluble sugars, vitamin C and free amino acids including gamma-aminobutyric acid (GABA) in spinach (*Spinacia oleracea*), Food Chem. 215 (2017) 185–192.
[64] F. Palma, F. Carvajal, J.M. Ramos, M. Jamilena, D. Garrido, Effect of putrescine application on maintenance of zucchini fruit quality during cold storage: contribution of GABA shunt and other related nitrogen metabolites, Postharvest Biol. Technol. 99 (2015) 131–140.
[65] M.T. Juergens, R.R. Deshpande, B.F. Lucker, J.-J. Park, H. Wang, M. Gargouri, F.O. Holguin, B. Disbrow, T. Schaub, J.N. Skepper, The regulation of photosynthetic structure and function during nitrogen deprivation in *Chlamydomonas reinhardtii*, Plant Physiol. 167 (2015) 558–573.
[66] X. Ma, J. Liu, B. Liu, T. Chen, B. Yang, F. Chen, Physiological and biochemical changes reveal stress-associated photosynthetic carbon partitioning into triacylglycerol in the oleaginous marine alga *Nannochloropsis oculata*, Algal Res. 16 (2016) 28–35.
[67] Y. Meng, J. Jiang, H. Wang, X. Cao, S. Xue, Q. Yang, W. Wang, The characteristics of TAG and EPA accumulation in *Nannochloropsis oceanica* IMET1 under different nitrogen supply regimes, Bioresour. Technol. 179 (2015) 483–489.
[68] E. da Costa, J. Silva, S.H. Mendonça, M.H. Abreu, M.R. Domingues, Lipidomic approaches towards deciphering glycolipids from microalgae as a reservoir of bioactive lipids, Mar. Drugs 14 (2016) 101.
[69] S. Li, J. Xu, J. Chen, J. Chen, C. Zhou, X. Yan, The major lipid changes of some important diet microalgae during the entire growth phase, Aquaculture 428 (2014) 104–110.
[70] S. Li, J. Xu, Y. Jiang, C. Zhou, X. Yu, Y. Zhong, J. Chen, X. Yan, Lipidomic analysis can distinguish between two morphologically similar strains of Nannochloropsis oceanica, J. Phycol. 51 (2015) 264–276.
[71] G.J. Martin, D.R. Hill, I.L. Olmstead, A. Bergamin, M.J. Shears, D.A. Dias, S.E. Kentish, P.J. Scales, C.Y. Botté, D.L. Callahan, Lipid profile remodeling in response to nitrogen deprivation in the microalgae *Chlorella* sp. (Trebouxiophyceae) and *Nannochloropsis* sp. (Eustigmatophyceae), PLoS One 9 (2014) e103389.
[72] S.A. Oradu, R.G. Cooks, Multistep mass spectrometry methodology for direct characterization of polar lipids in green microalgae using paper spray ionization, Anal. Chem. 84 (2012) 10576–10585.
[73] H. Jiang, K. Gao, Effects of lowering temperature during culture on the production of polyunsaturated fatty acids in the marine diatom *Phaeodactylum tricornutum* (Bacillariophyceae), J. Phycol. 40 (2004) 651–654.
[74] I. Khozin-Goldberg, H.Z. Yu, D. Adlerstein, S. Didi-Cohen, Y.M. Heimer, Z. Cohen, Triacylglycerols of the red microalga *Porphyridium cruentum* can contribute to the biosynthesis of eukaryotic galactolipids, Lipids 35 (2000) 881–889.
[75] T. Tonon, D. Harvey, T.R. Larson, I.A. Graham, Long chain polyunsaturated fatty acid production and partitioning to triacylglycerols in four microalgae, Phytochemistry 61 (2002) 15–24.
[76] J. HARWOOD, A. OKANENKO, Sulphoquinovosyl diacylglycerol (SQDG) the sulpholipid of higher plants, Sulphur in Plants, 189 2003.
[77] S. Naoki, M. Norio, M. Yoshiro, U. Nobuo, Effect of growth temperature on lipid and fatty acid compositions in the blue-green algae, *Anabaena variabilis* and *Anacystis nidulans*, Biochim. Biophys. Acta, Lipids Lipid Metab. 572 (1979) 19–28.
[78] K.P. Quoc, J.-P. Dubacq, Effect of growth temperature on the biosynthesis of eukaryotic lipid molecular species by the cyanobacterium Spirulina platensis, Biochim. Biophys. Acta, Lipids Lipid Metab. 1346 (1997) 237–246.
[79] H. Wada, N. Murata, Membrane Lipids in Cyanobacteria, Lipids in Photosynthesis: Structure, Function and Genetics, Springer, 1998, pp. 65–81.